Atom Probe and Transmission Electron Microscopy Investigations of Heavily Drawn Pearlitic Steel Wire

M. H. HONG, W. T. REYNOLDS, JR., T. TARUI and K. HONO

Transmission electron microscopy (TEM) and atom probe field ion microscopy (APFIM) observations of pearlitic steel wire show drawing to a true strain of 4.22 causes fragmentation of cementite lamella into nanoscale grains. The drawing strain amorphizes some portions of the cementite lamella in regions where the interlamellar spacing is very small, but most of the cementite lamella are polycrystalline with nanoscale grains. The carbon concentration in the ferrite is inhomogeneous and varies from 0.2 to 3 at.%; the carbon concentration in nanocrystalline cementite is less than 18 at.%, significantly lower than in stoichiometric Fe_3C. Silicon is segregated to ferrite/cementite boundaries, but in regions with a small interlamellar spacing, the silicon concentration is uniform across the lamella. Annealing at 200°C for 1 hr does not cause noticeable changes in the microstructure. Annealing at 400°C or above for 1 hr causes spherodization of the cementite lamella, and the carbon concentrations in ferrite and in cementite return to the pre-deformation values.

I. INTRODUCTION

HEAVILY drawn pearlitic wire has been investigated extensively over the years for its unusual strain-hardening behavior and for the high strengths that can be attained with toughness sufficient for many engineering applications[1]. Widely used for tire cord, springs, wire rope, and suspension bridge cable, it is typically produced by rolling or drawing wire of approximately eutectoid composition to an intermediate diameter, patenting to produce a fine pearlitic microstructure, and then cold drawing to strains between 1.5 and 5.0. Previous microstructural investigations have established a number of salient characteristics associated with the wire drawing process[2,3,4]. The strength of the wire increases exponentially with drawing strain, and despite the limited ductility of monolithic cementite crystals[5,6,7,8], the cementite lamella in pearlitic wire co-deform with ferrite. The ferritic component develops a strong <110> wire texture,[9] and the cementite lamella appear to fragment into planar arrays of small particles[3,10,11]. No preferred texture has been identified for the cementite phase. The pearlite interlamellar spacing decreases in proportion to the wire diameter, and the range of spacings broadens markedly with increasing strain.[3]

In addition to these microstructural traits, drawn pearlitic wire has several interesting chemical characteristics. Atom probe field ion microscopy (APFIM) [12,13,14,15,16] studies indicate silicon in undeformed (as-patented) wire is piled-up at ferrite/cementite boundaries while manganese shows no significant tendency to segregate or partition to either ferrite or cementite. Internal friction[17] and Mössbauer[18] experiments suggest a substantial proportion of the cementite (from 20 to 50 volume percent) dissolves during deformation at room temperature. This phenomenon is intriguing since cementite is stable at room temperature and the solubility of carbon in ferrite is quite low. Direct support for cementite dissolution is provided by the aforementioned APFIM investigations [12,13,14,15,16] as well as several analytical transmission electron microscopy (TEM) [11,19] studies that show deformed ferrite lamella contain significantly more carbon than ferrite in undeformed pearlite.

Explanations for why cementite dissolves during cold drawing are based upon either interactions between carbon and dislocations or upon thermodynamic arguments. In the first category, Gridnev et al.[18] suggested a larger binding energy between interstitials and dislocations in ferrite than between carbon and cementite makes it possible for dislocations to drag carbon out of cementite. Others suggested cementite dissolves during annealing when carbon leaves cementite to form atmospheres around dislocations in ferrite[17]. In the second category, Languillaume et al. [11] invoked capillarity to argue an increase in surface energy associated with steps in pearlite lamella destabilizes the cementite phase.

The distribution of carbon in deformed pearlitic wire is important as it affects the response of drawn wire to subsequent thermal treatments. Commercial pearlitic wire is often heat treated at temperatures ranging from 200 to 450°C during bluing or galvanizing processes, and the mechanisms associated with observed changes in mechanical properties depend on the behavior of carbon after drawing. For example, the increase in yield strength that results from brief exposures to temperatures below approximately 250°C has been attributed to strain-age hardening accompanying cementite dissolution[17]. Also, the softening accompanying annealing at higher temperatures has been attributed to a variety of processes including a drop in the carbon

M. H. HONG, JST fellow, and K. HONO, Head of Laboratory, are with Materials Physics Division, National Research Institute for Metals, 1-2-1 Sengen, Tsukuba 305-0047, Japan. W. T. REYNOLDS, JR., Associate Professor, is with Materials Science and Engineering Department, Virginia Tech., Blacksburg, VA 24061-0237, U.S.A. T. TARUI, Senior Researcher, is with Steel Research Laboratories, Nippon Steel Corporation, Futtsu, 293-0011, Japan.

Manuscript submitted March 4, 1998.

concentration in ferrite[16], recovery and recrystallization[20], and cementite spherodization[11,20].

The present study aims to clarify the mechanism by which carbon is transferred from cementite to pearlite during deformation as well as to determine how annealing between 200 and 500°C affects the distribution of carbon and silicon. Toward this end, three-dimensional APFIM and TEM techniques were used to obtain both chemical and microstructural information with spatial resolutions of near-atomic dimensions.

II. EXPERIMENTAL PROCEDURES

The material used in this investigation was commercial tire cord wire provided by Nippon Steel Corporation. This carbon steel was of approximately eutectoid composition (Fe-0.82C-0.5Mn-0.25Si wt.% or Fe-3.69C-0.49Mn-0.48Si at%). The alloy was vacuum induction melted, cast into ingots, hot forged, and hot rolled into wire rod 1.65 mm in diameter before final patenting. Patenting consisted of austenitizing at 950°C for 1800 sec followed by isothermal transformation for 30 sec in a lead bath at 560°C. The patented wire was subsequently cold-drawn in multiple dies to a final diameter of 0.2 mm which corresponds to a true strain of 4.22. * The yield strength and tensile strength of the wire was 3,600 and 3,933 MPa, respectively. To study the effects of isothermal annealing, wires were aged at temperatures between 200 and 500°C for 1 hr and quenched in water. The annealing treatments were carried out in either an oil bath (below 200°C) or a salt bath (above 250°C).

*The true strain, ε, is defined as $\ln(A_i/A_f)$, where A_i and A_f are the initial and final cross-sectional areas of the wire.

TEM observations were made along two directions in the wire: a longitudinal view in which the electron beam was oriented perpendicular to the wire axis, and a cross sectional view in which the electron beam was parallel to the wire axis. Longitudinal TEM specimens were mechanically ground to a thickness of about 60 μm and electropolished in 10% perchloric acid in ethanol. Cross sectional TEM specimens were made by placing 0.2 mm diameter wire in a 3 mm diameter copper tube and filling the remaining space with epoxy. The resulting composite was sectioned with a diamond saw, mechanically thinned and dimpled to a thickness of 15 μm, and finally thinned to electron transparency with a Fischione Model 3000 ion mill using an ion energy of 4 kV and ion current of 4.0 mA. The thin-foil specimens were examined with a Philips* CM200 TEM operated at a 200kV accelerating voltage and with JEOL* JEM-2000EX and 4000EX microscopes operated at 200 and 400 kV, respectively.

*PHILIPS is a trademark of Philips Electronic Instruments Corp., Mahwah, NJ.

*JEOL is a trademark of Japan Electron Optics Ltd., Tokyo.

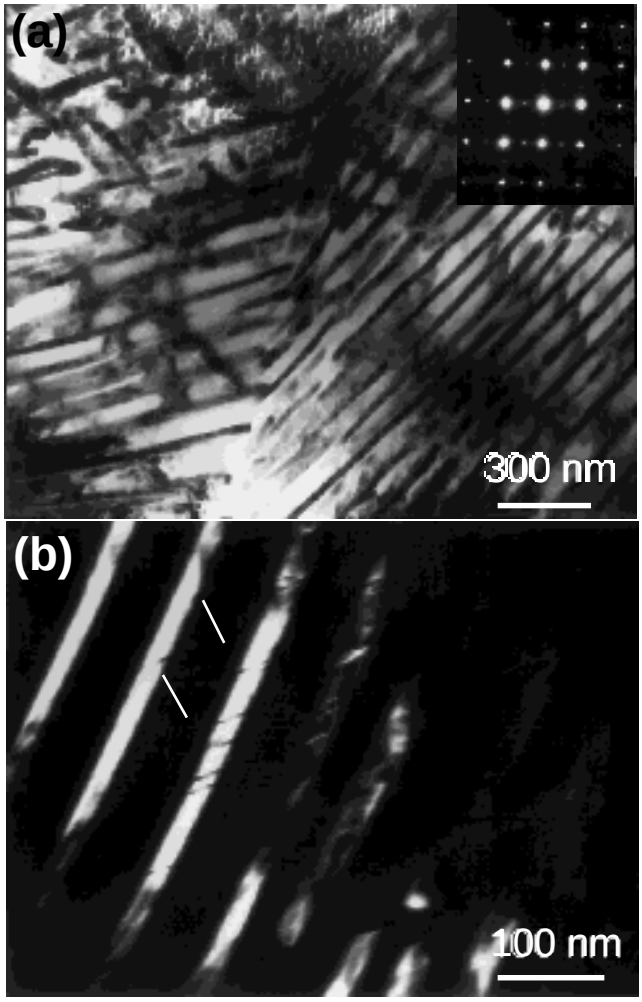

Fig. 1----Cross sectional (a) bright-field and (b) dark-field images of patented pearlitic wire. The beam direction is close to the [001] zone of ferrite. The image in (b) was obtained using the cementite reflection circled in (a).

The APFIM specimens were prepared using a two-stage electropolishing procedure. Wires were first thinned in a solution of 25% perchloric acid and 75% acetic acid at 30V DC, then micro-electropolished in 2% perchloric acid and 98% Butoxyethanol at 20 V DC.

The three-dimensional atom probe (3DAP) instrument used in this study was equipped with CAMECA's tomographic atom probe (TAP) detection system installed on a locally-built field ion microscope (FIM). Details of the TAP detector system are described elsewhere[21]. FIM images were observed using Ne at tip temperatures ranging from 20 to 60 K (usually close to 60 K). The atom probe analyses was carried out in ultra-high vacuum (~1 x 10^{-8} Pa) with a 0.2 pulse fraction (ratio of pulse voltage to static voltage, V_p/V_{dc}) at tip temperatures in the range of 30 - 60 K. Visualization and analysis of 3DAP data were carried out using Kindbrisk SDV 3DAP data analysis software running on the Advanced Visualization System (AVS).

It is difficult to differentiate manganese from iron with the 3DAP system employed for this study because the ion

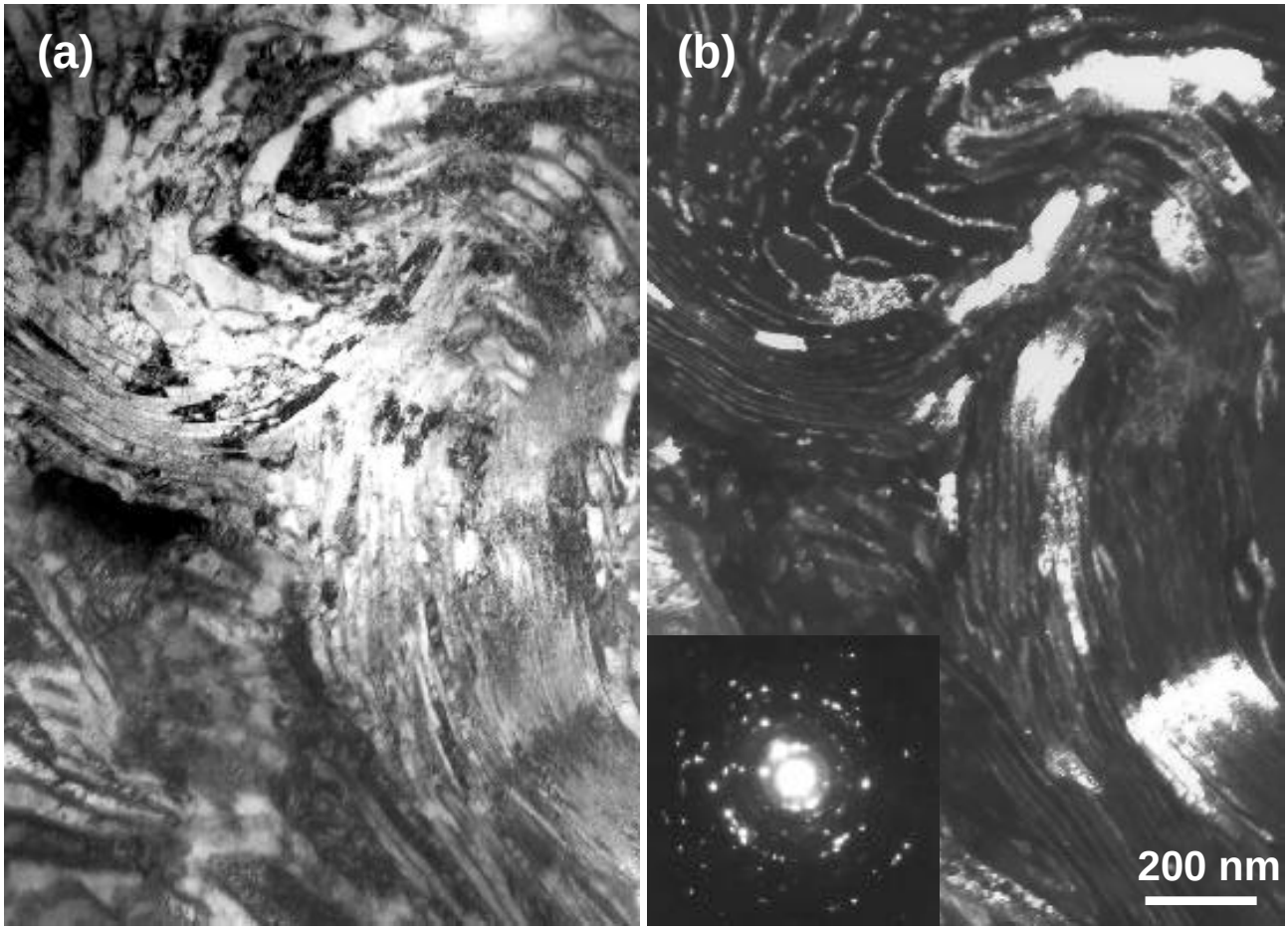

Fig. 2–––Cross sectional (a) bright-field and (b) dark-field images of wire drawn to a true strain of 4.22. The selected area diffraction pattern (inset) includes sharp ferrite reflections as well as ring patterns. The cementite reflection used for the dark-field image is circled.

mass spectra of Mn^{++} (27.5 amu) and Fe^{++} (27 and 28 amu) overlap. However, previous one-dimensional atom probe results from the same material[16] showed the manganese concentration is uniform in both as-patented and deformed wire, so the comparatively small amount of manganese was included together with the Fe component in the 3DAP analysis. Silicon peaks in the mass spectrum occur between m/n=14-15 and there is no ambiguity in distinguishing them from iron, assuming that all silicon atoms are ionized as doubly charged ions. Detected carbon peaks were found at mass-to-charge ratios of 6 (C^{++}) and 12 (C^{+} and C_2^{++}), 18 (C_3^{++}), 24 (C_2^{+} and C_4^{++}) and 36 (C_3^{+}). In this study, the carbon concentration was calculated by assuming the m/n=12 peak results entirely from C^{+} (a negligible contribution from C_2^{++}), and the ions at the m/n=24 peak are C_2^{+}.

III. RESULTS

A. *Transmission Electron Microscopy*

Figure 1 shows bright field and dark field TEM micrographs of the as-patented wire in cross sectional view with the electron beam nearly parallel to the [001] ferrite zone. The dark field image in Figure 1 (b) was obtained using the cementite reflection circled in the inset to Figure 1 (a). The interlamellar spacing is uniform within a given colony (approximately 130 nm) and the thickness of the cementite lamella is about 20 nm. Strain contrast is commonly observed in the ferrite lamella, and planar defects can also be found in the cementite lamella (indicated by arrows in Figure 1 (b)). The latter appear much like the stacking faults and slip traces seen in pearlitic cementite deformed to low strains[5,6,7,8]. These observations indicate there is some internal strain in the as-transformed pearlite.

Figure 2 shows cross sectional TEM micrographs of a wire drawn to a true strain of 4.22. The pearlite lamella exhibit a characteristic curled morphology first described by Langford[3], and it is evident the interlamellar spacing varies substantially from one ferrite grain to another. In contrast to the single crystal lamella found in undeformed pearlite, the dark field image of the heavily deformed pearlite (Figure 2(b)) shows the cementite lamella are fragmented into small grains. Individual dislocations are not resolvable at this large strain, but strain contrast (at arrows in Figure 3(a)) are found throughout the ferrite lamella. These are

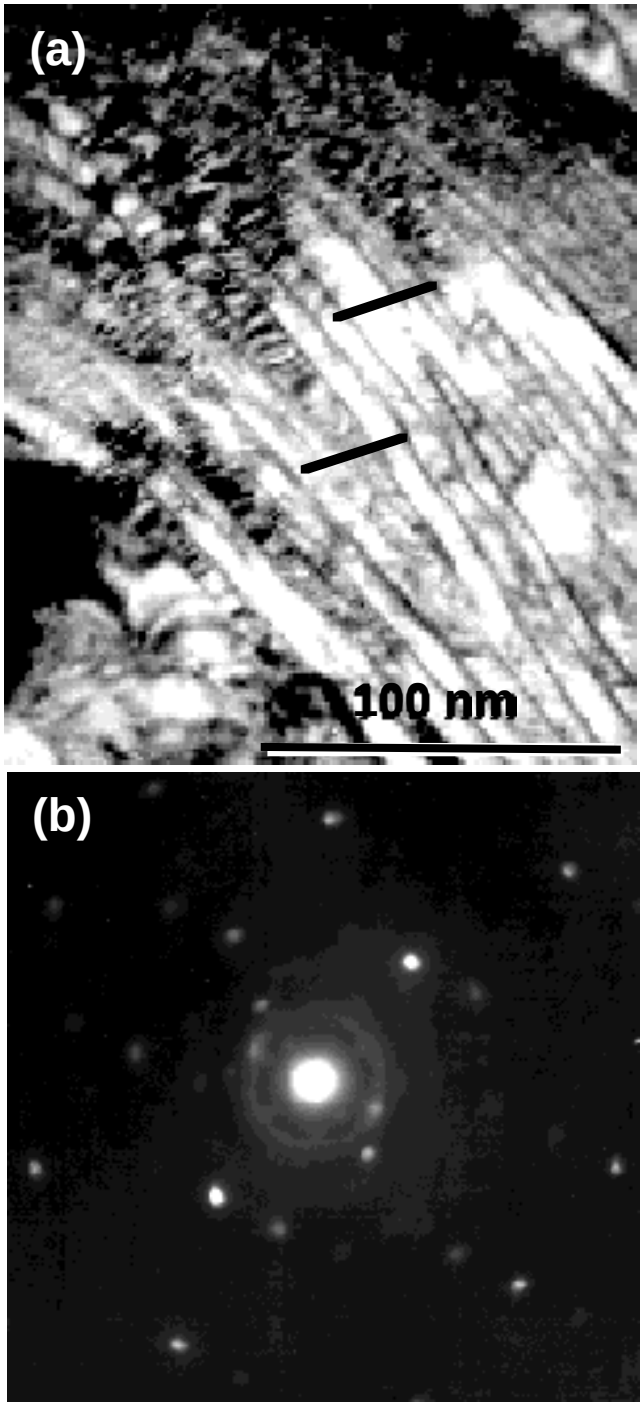

Fig. 3———(a) Contrast arising from regions of local strain (arrowed) found throughout the ferrite lamella. (b) A diffuse halo obtained with microdiffraction from a highly deformed cementite lamella. The true strain in the wire is 4.22.

believed to arise from regions in ferrite with relatively high dislocation densities. Selected area diffraction patterns, such as the inset in Figure 2(b), include fairly sharp ferrite reflections as well as rings corresponding to cementite interplanar spacings. Using microdiffraction with a nominal probe size of 5 nm, it was concluded the rings result from small, randomly oriented fragmented cementite grains. Thus, the fragmented appearance of the cementite in the dark field image of Figure 2(b) comes from imaging only a small portion of the randomly oriented grains.

Occasionally, a diffuse halo was observed in microdiffraction patterns from regions where the interlamellar spacing was particularly small (~ 10 nm) as shown in Figure 3 (b). There are several possible explanations for such a halo. A number of diffracting planes in cementite have similar interplanar spacings, so randomly oriented cementite grains could give rise to a halo. This explanation does not account well for the uniformity of the halo in Figure 3 (b) given the small volume sampled by the electron beam - a cylinder through the foil not much larger than 5 nm in diameter. Alternatively, the halo could arise from an oxide layer on the foil. Although this possibility cannot be ruled out, the fact that the halo was only observed at the thinnest of the cementite lamella suggests it comes from an amorphous-like structure in regions of cementite that underwent the greatest deformation.

An HREM image taken from a region with a small interlamellar spacing is shown in Figure 4. The large plastic strain in the wire made it difficult to obtain clear zone-axis patterns from either ferrite or cementite, but lattice fringes could still be obtained at various locations. The horizontal bands in the micrograph correspond to two cementite lamella. The fringes in these lamella and the discrete spots in Fourier transforms of cementite regions (e.g., inset at bottom center of Figure 4) indicate most of the cementite is crystalline. Individual grains between 5 and 10 nm can be seen within cementite lamella in agreement with recent results reported by Languillaume[11]. The absence of clear spots in the Fourier transform obtained from the left inset in Figure 4 suggests this particular portion of the cementite may be amorphous. The discontinuous nature of the two cementite lamella in Figure 4 is worth noting. The upper lamella appears to terminate in the middle of the figure (it actually continues left of the region shown in the micrograph) and the lower one has a break where there is strong strain contrast in ferrite. Although termination of cementite lamella are common in undeformed pearlite, they are more common in drawn wire and are usually associated with strained regions in ferrite. No evidence was found for cracks in cementite, so the thinning and termination of the lamella evidently occurred through plastic deformation.

Figure 5 shows the effect of various annealing treatments on the microstructure of the wire in longitudinal view. Annealing the wire at 200°C for 1 hr has little effect on the appearance of the microstructure. Figures 5 (a) and (b) are of as-drawn wire, and (c) and (d) are from wire annealed at 200°C for 1 hr. There are no appreciable differences between as-drawn wire and wire annealed at 200°C for 1 hr. Strain contrast is still present in the ferrite lamella after annealing at 200°C (Figure 5(c)), and the cementite still has a fragmented nanocrystalline structure (Figure 5(d)).

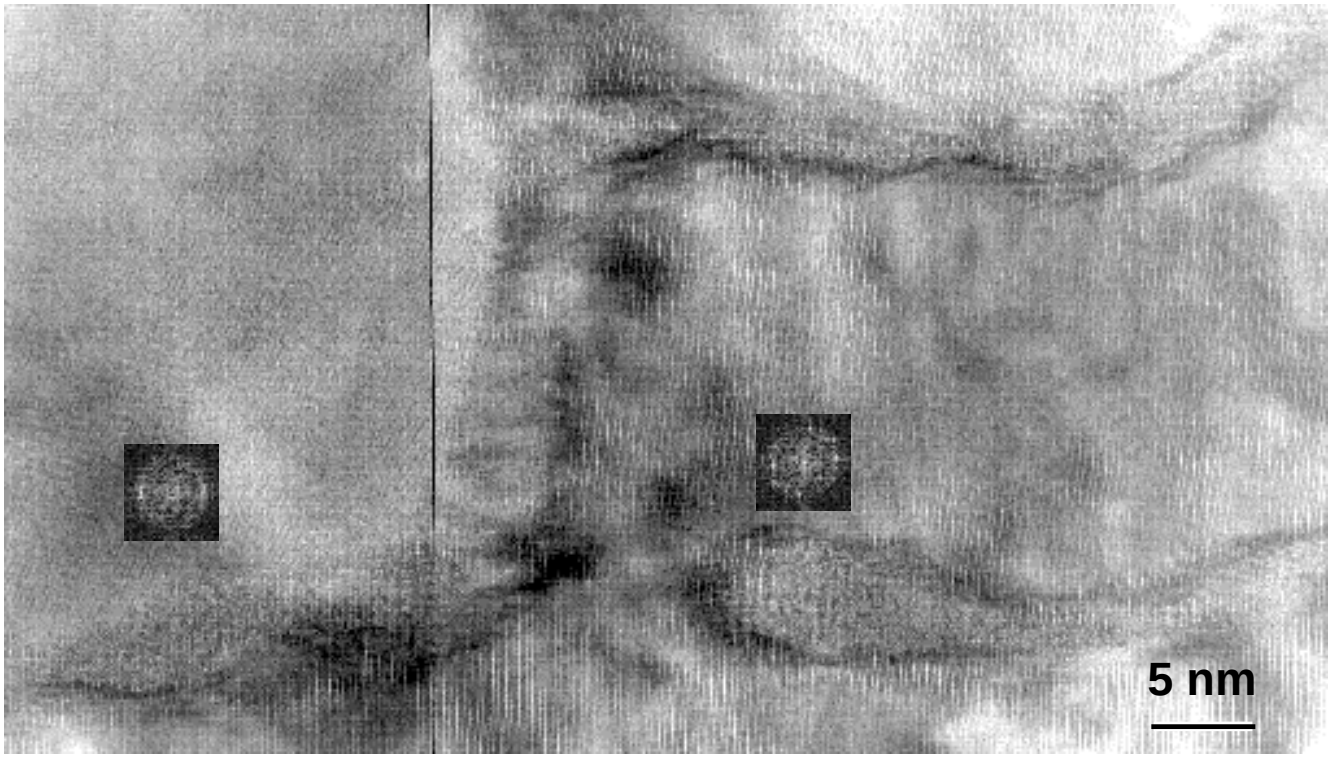

Fig. 4----A high-resolution TEM image taken from a region of deformed pearlite with a particularly small interlamellar spacing (the true strain is 4.22). The horizontal bands in the micrograph correspond to two cementite lamella.

Substantial microstructural changes take place during annealing at 400°C for 1hr (Figures 5 (e) and (f)). The lamellar microstructure is still present, but the interlamellar spacing appears coarser than in the as-drawn wire. The cementite lamella are no longer continuous, and coarsened cementite grains 20-30 nm in diameter are observed even within the ferrite lamella. Some of the cementite grains have coarsened to between 50 and 70 nm in diameter, arrowed in Figure 5(f). Figures 5 (g) and (h) show bright field and dark field images of wire annealed at 500°C for 1 hr. The lamellar structure is completely destroyed by recrystallization of ferrite and spherodization of cementite. Strong strain contrast in ferrite is no longer evident.

B. *Atom Probe Field Ion Microscopy*

Figures 6 (a) and (b) show 3DAP carbon maps in as-patented and in as-drawn wire, respectively. The dimensions of the analyzed volumes are approximately 18 × 18 × 24 nm in 6(a) and 18 × 18 × 21 nm in 6(b). Each dot represents a location at which a carbon specie was detected (ionized C, C_2, C_3, or C_4); all other elements are omitted for clarity. The regions in Figure 6 with a relatively high density of carbon ions extending from the top to the bottom of the analyzed volumes correspond to cementite lamella. Ferrite is easily identified by its comparatively low density of carbon atoms. The undeformed cementite lamella in Figure 6 (a) is approximately 20 nm thick, and the deformed cementite lamella in Figure 6 (b) are 5 nm thick in good agreement with thicknesses measured with TEM (Figures 1, 2 and 5).

Local composition information can be obtained by analyzing data extracted from a small "selected" volume within a 3DAP analysis region. The selected volume can be chosen to provide elemental maps, concentrations, or concentration profiles along a direction within the 3DAP analysis region. For clarity, the larger 3DAP analysis regions are omitted from subsequent figures and only the selected volumes are shown. Figure 7 (a) shows 3DAP elemental maps of carbon and silicon from the selected volume outlined by the small box in Figure 6 (a). The orientation of the selected volume was chosen to reveal the carbon and silicon concentration profiles perpendicular to the pearlite lamella. The left side of Figure 7 (a) corresponds to a ferrite lamella in undeformed pearlite, and the right side corresponds to cementite. Under ideal conditions, the 3DAP is capable of positioning atoms in the analyzed volume with an accuracy of about 0.2 nm. However, preferential evaporation of cementite causes aberrations in the electric field that degrade the spatial resolution of the instrument. Errors in positioning atoms in the present experiments are estimated to be less than 1 nm based on the abrupt change in carbon concentration at the ferrite/cementite boundary from undeformed pearlite shown in Figure 7 (a).

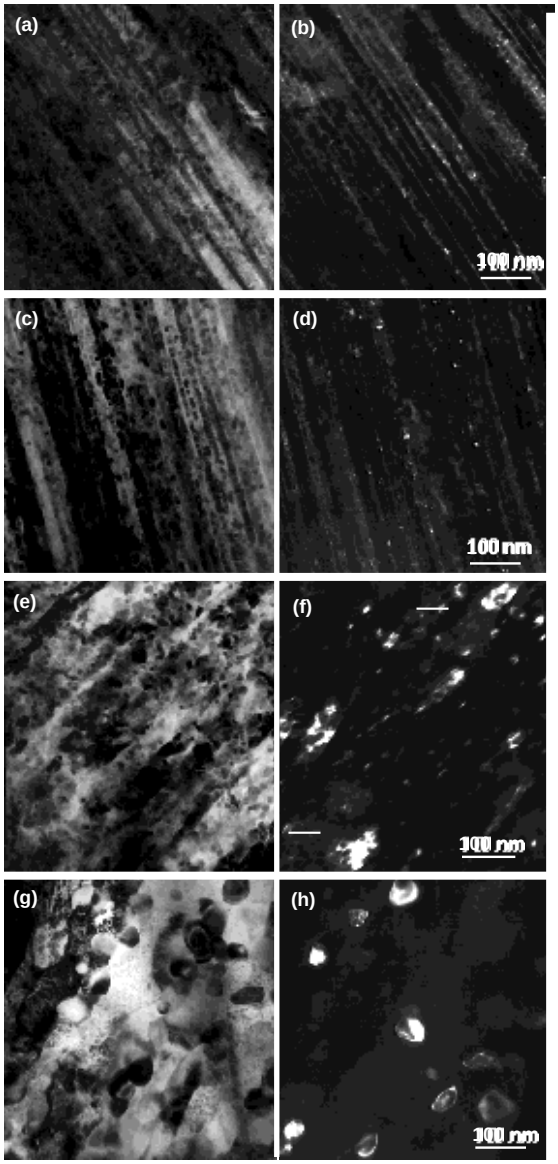

Fig. 5----The effect of annealing on the microstructure of pearlitic wire drawn to a true strain of 4.22. Bright-field/dark-field pairs taken perpendicular to the wire axis (longitudinal view): as-drawn wire (a) and (b); annealed at 200°C for 1 hr (c) and (d); annealed at 400°C for 1 hr (e) and (f); annealed at 500°C for 1 hr (g) and (h).

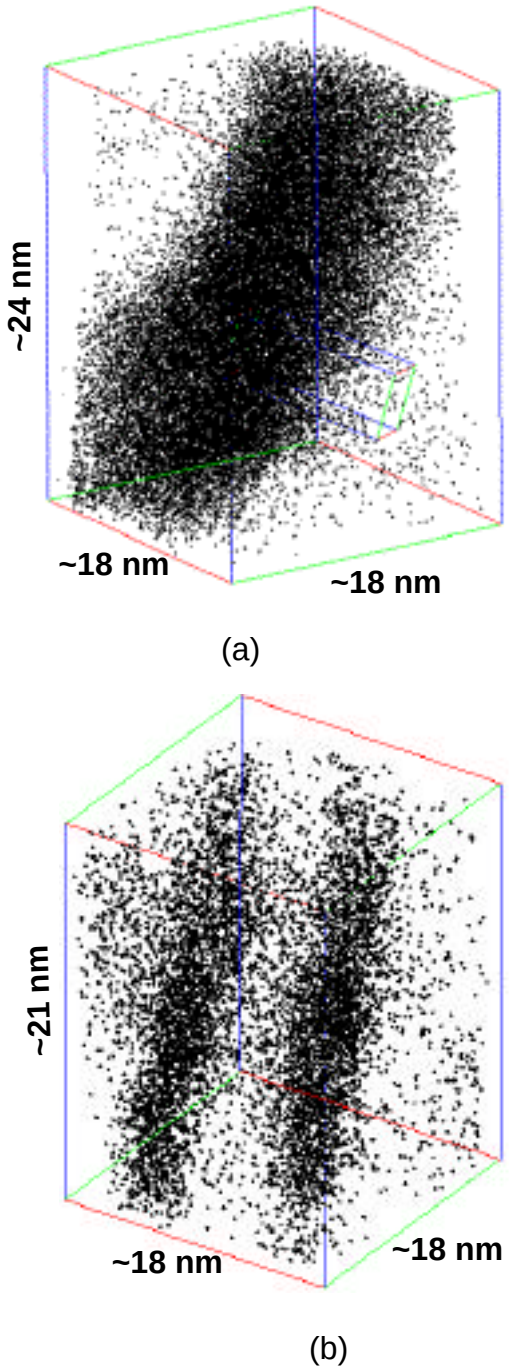

Fig. 6----- 3DAP carbon maps of (a) undeformed and (b) deformed pearlitic wires. Each dot represents the location at which a carbon ion was detected.

Figure 7 (b) shows concentration depth profiles of carbon and silicon calculated from the same selected volume used in Figure 7 (a). Two factors affect the accuracy of the calculated concentrations: systematic errors associated with instrumental parameters and sampling statistics. An estimate of the systematic errors can be obtained from the measured carbon concentration in undeformed cementite; this value is approximately 24 at.% (Figure 7 (b)), which is in good agreement with the expected stoichiometry of carbon in cementite (25 at.%). Thus, the carbon concentrations determined from atom probe data are accurate to within a factor of approximately 0.05. Uncertainties arising from sampling statistics decrease with the number of atoms used to calculate the concentrations. However, increasing the sample volume to improve the statistical accuracy sacrifices the spatial resolution of the measurement. Concentration profiles like the ones in Figure 7 (b) were determined using a moving average to strike a balance

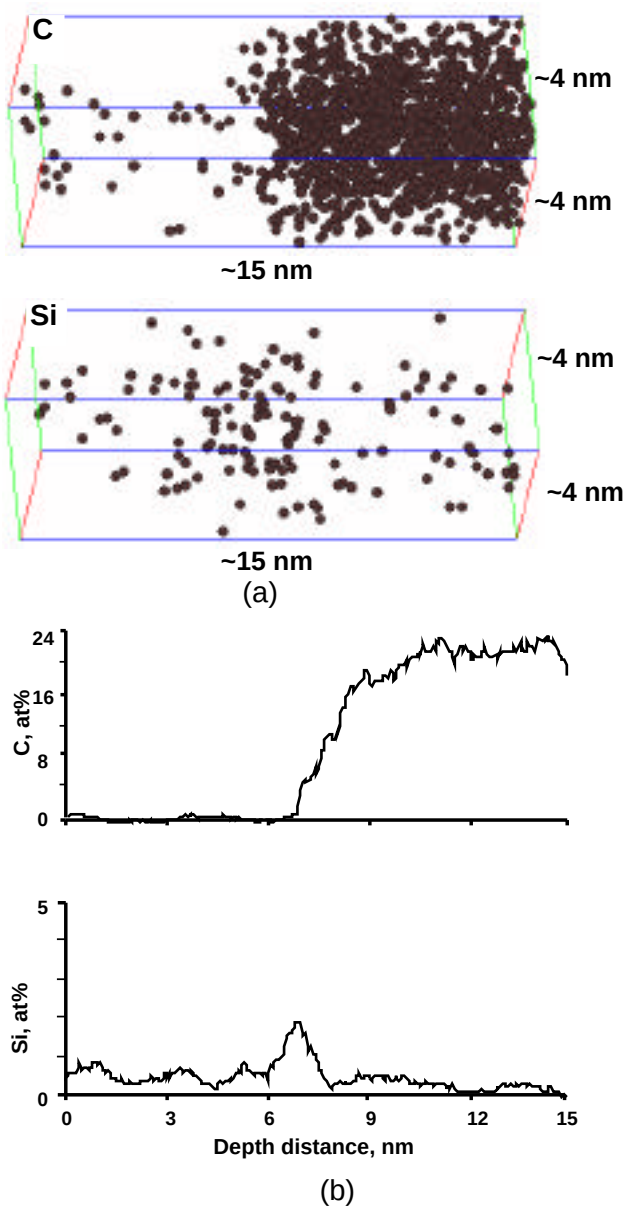

Fig. 7----- (a) 3DAP elemental maps of carbon and silicon in the selected volume outlined in Figure 6 (a). (b) Carbon and silicon concentration profiles obtained from (a); each nanometer of distance roughly corresponds to 1000 atoms.

between statistical confidence and spatial detail. At each depth distance, the concentrations were calculated by counting all the species in a block consisting of a layer 0.5 nm thick times the width and height of the selected volume. A typical block contained about 500 atoms, and the concentration profiles were obtained by moving the position of the block from one end of the selected volume to the other. The concentrations vary by a factor of about 0.15 from one depth to the next, and this "noise" is not statistically significant. Larger concentration fluctuations extending over a depth of a couple nanometers reflect

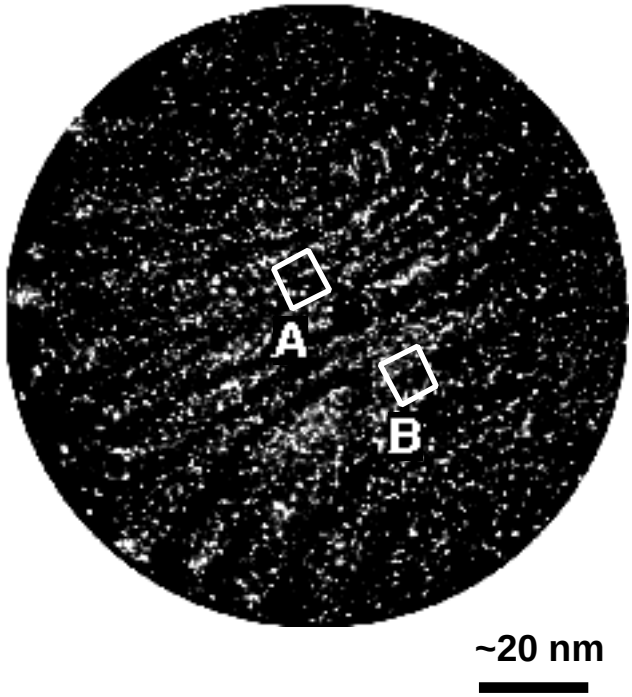

Fig. 8----- A Ne field ion image of wire drawn to a true strain of 4.22. The brightly imaging bands are ferrite lamella, and darkly imaging bands are cementite lamella. Regions at A and B were analyzed by 3DAP.

significant concentration variations involving several thousand atoms.

In Figure 7 (b), the carbon concentration in ferrite is estimated to be 0.07 at.%, perhaps a little higher than the equilibrium carbon concentration at 560°C, i.e. 0.01 at.%. This result indicates the ferrite in patented pearlitic wire does not reach equilibrium and is slightly supersaturated with carbon[13,16] after patenting at 560°C for 30 sec. The ferrite/cementite boundary is relatively sharp and silicon appears to be enriched to a concentration of approximately 2 at.% at the boundary.

Figure 8 shows a field ion micrograph of a wire drawn to a true strain of 4.22; the wire axis is perpendicular to the plane of the figure. The brightly imaging bands are ferrite lamella, and the dark bands correspond to cementite lamella. In order to determine carbon concentrations in ferrite and in cementite, two selected volumes located at A and B were analyzed by 3DAP.

Figure 9 (a) shows 3DAP elemental maps of carbon and silicon in a selected volume 4 × 4 × 15 nm in size obtained from region where the interlamellar spacing is very small (location A in Figure 8). The two cementite lamella are resolved along the analysis direction. The location of cementite and ferrite can be recognized by the difference in the density of carbon. Carbon-enriched regions correspond to cementite lamella and some carbon atoms appear to be present even in the ferrite region. The ferrite/cementite interface appears diffuse, but this may be due in part to evaporation aberration of ions originating from surfaces

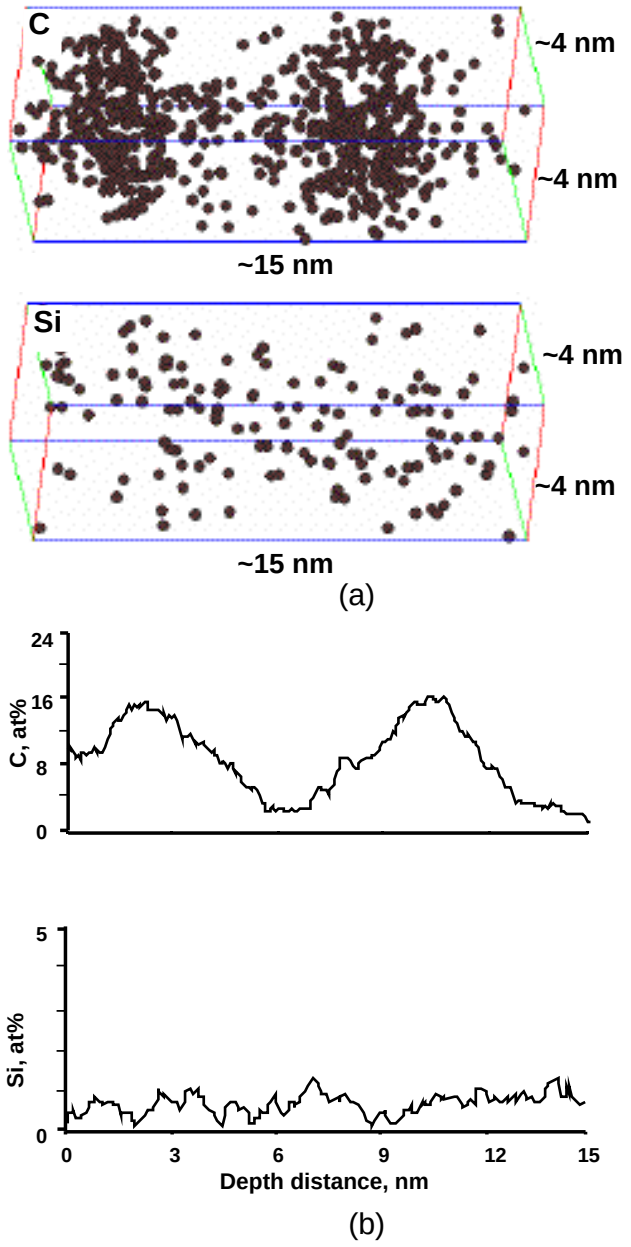

Fig. 9----- (a) 3DAP elemental maps of carbon and silicon obtained from region A in Figure 8. (b) The corresponding carbon and silicon concentration profiles across the ferrite/cementite interface. Each nanometer of distance roughly corresponds to 1000 atoms.

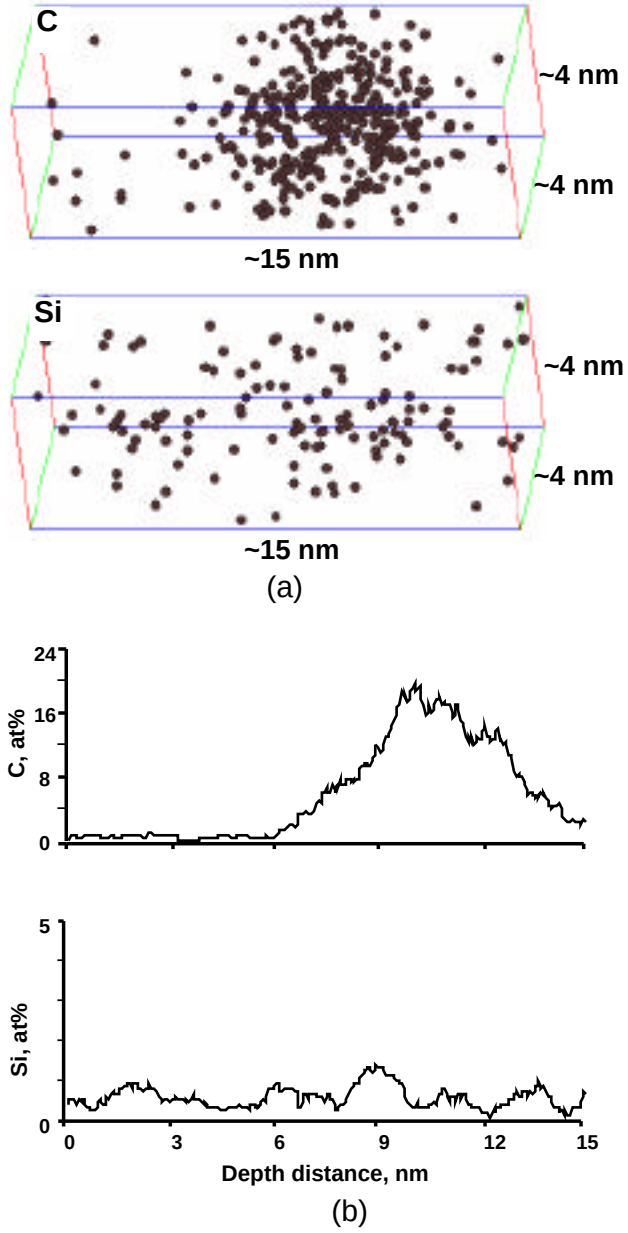

Fig. 10---- (a) 3DAP elemental maps of carbon and silicon obtained from region B in Figure 12. (b) The corresponding carbon and silicon concentration profiles across the ferrite/cementite boundary. E); each nanometer of distance roughly corresponds to 1000 atoms.

with slightly different local curvatures. The corresponding concentration profiles are shown in Figure 9 (b). The carbon concentration in cementite is approximately 16 at.%, considerably lower than the stoichiometry of cementite (25 at.% C). On the other hand, the carbon concentration in the ferrite ranges from 2 to 3 at.% and is significantly higher than that observed in as-patented ferrite. This type of analysis was repeated several times, and a 2-3 at.% carbon concentration in ferrite was reproducibly recorded. In the heavily deformed wire, silicon enrichment at the ferrite/cementite interface is not observed in regions with a small interlamellar spacing, Figure 9 (b). This result indicates that silicon also undergoes some mixing during the wire drawing process.

Figure 10 (a) shows a set of carbon and silicon maps obtained from location B in Figure 8. The interlamellar spacing in this region is somewhat coarser than that of location A. Consequently, only one cementite lamella is included within the selected volume. The carbon concentration in ferrite in Figure 10 (b) is between 0.2 and 1 at.%, and is considerably lower than that observed in ferrite with a finer interlamellar spacing (c.f. 2 to 3 at.%).

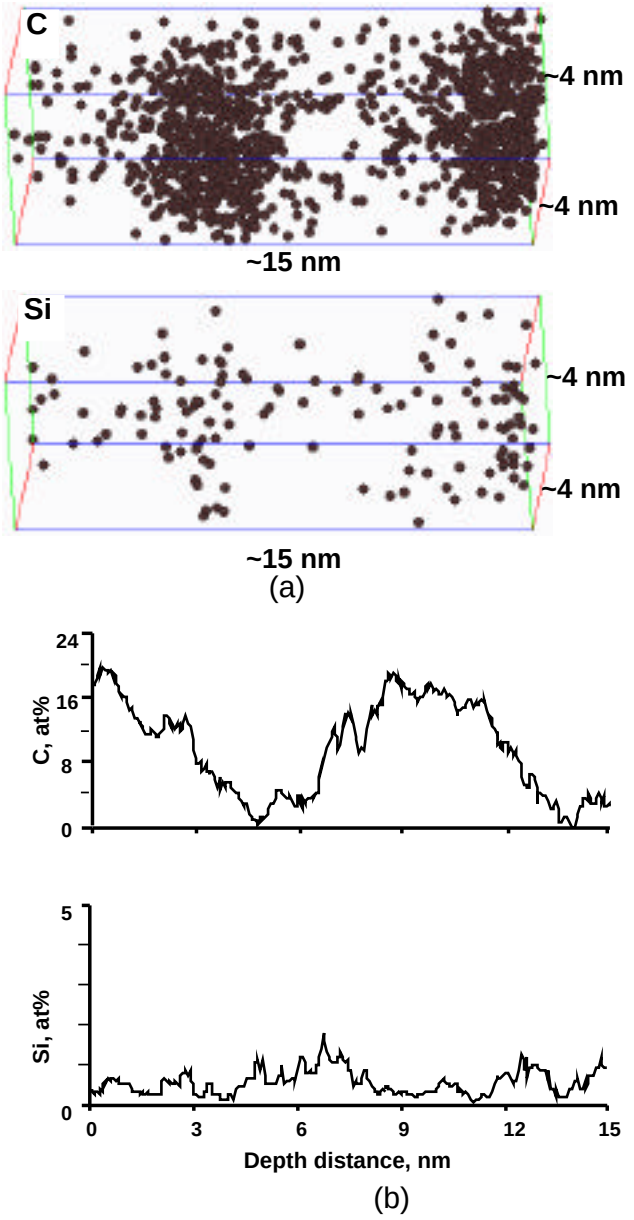

Fig. 11---- (a) 3DAP elemental maps of carbon and silicon in a pearlitic wire (ε=4.22) aged at 200°C for 1hr. (b) The corresponding carbon and silicon concentration profiles across the ferrite/cementite interface in (a). Each nanometer of distance roughly corresponds to 1000 atoms.

This result indicates the carbon concentration in heavily drawn wire is very inhomogeneous, and it is higher where the interlamellar spacing is smaller. The silicon profile in Figure 10 suggests there is some silicon enrichment at the ferrite/cementite interface.

A 3DAP elemental maps of carbon and silicon obtained from a wire drawn to ε=4.22 and aged at 200°C for 1hr (Figure 11) are qualitatively the same as those of the as-drawn wire (Figure 9); there is still a substantial amount of excess carbon dissolved in the ferrite lamella and the carbon concentration in cementite is still significantly lower than stoichiometric Fe_3C. There appears to be a tendency for some silicon enrichment at the ferrite/cementite boundaries.

An FIM image of wire aged at 400°C for 1 hr is shown in Figure 12 (a). The brightly imaging regions are ferrite, and cementite lies within the narrow, dark bands. The interlamellar spacing is greater than in as-drawn wire, in agreement with the TEM results shown in Figure 5. The concentric rings of the low index planes in ferrite are imaged more clearly than in as-drawn wire (Figure 8), implying the ferrite lattice has become less distorted, presumably from less dissolved carbon. Such clear FIM images of ferrite are typical for low alloy ferritic steels.

Figure 12 (b) shows 3DAP elemental maps of carbon and silicon in a wire aged at 400°C for 1 hr; these conditions spherodize the cementite (refer to Figure 5). The ferrite/cementite boundary is clearly delineated by the carbon distribution. Figure 12 (c) shows the corresponding concentration profiles of carbon and silicon calculated from the selected volume. The carbon concentration in the cementite is approximately 24 at.% and that in ferrite is 0.07 at.%; these values are similar to those obtained from the as-patented (undeformed) wire. Enrichment of silicon is observed at the ferrite/cementite interface, where the silicon concentration is approximately 2 at.%. These results suggest spherodization of cementite at 400°C is accompanied by recovery and/or recrystallization of ferrite and a loss of the excess carbon in ferrite.

IV. DISCUSSION

The most interesting result of the 3DAP analyses is the direct evidence for cementite dissolution during cold-drawing. In wire drawn to a strain of 4.22, the average carbon concentration in ferrite is approximately 2 at.%C, but the local concentration varies between 0.2 and 3 at.%. In addition, when ferrite regions exhibiting particularly clear FIM images are analyzed by atom probe, they invariably contain low levels of carbon, and regions with distorted FIM images contain higher carbon concentrations. This demonstrates that carbon is not dissolved in ferrite uniformly, but is probably bound to dislocations. TEM results suggest the dislocation density in ferrite is not uniform after deformation of ε=4.22. Thus, the strong binding of carbon to dislocations is a likely cause of the increase in the apparent carbon concentration in ferrite, and we conclude carbon segregates to dislocations or dislocation pile-ups in ferrite rather than dissolving in ferrite as a uniform solid solution.

Previous Mössbauer[17] and HREM studies[11] suggested cementite dissolution occurs during heavy deformation, and the corresponding increase in carbon content in ferrite is expected. The Mössbauer work reported 20 to 50% of the cementite can dissolve during cold work. 50% dissolution of the equilibrium fraction of cementite in pearlitic steel of eutectoid composition requires an increase in the carbon concentration in ferrite up to about 2.7 at%. Thus, the 2 to 3 at.% carbon concentration in ferrite observed in this

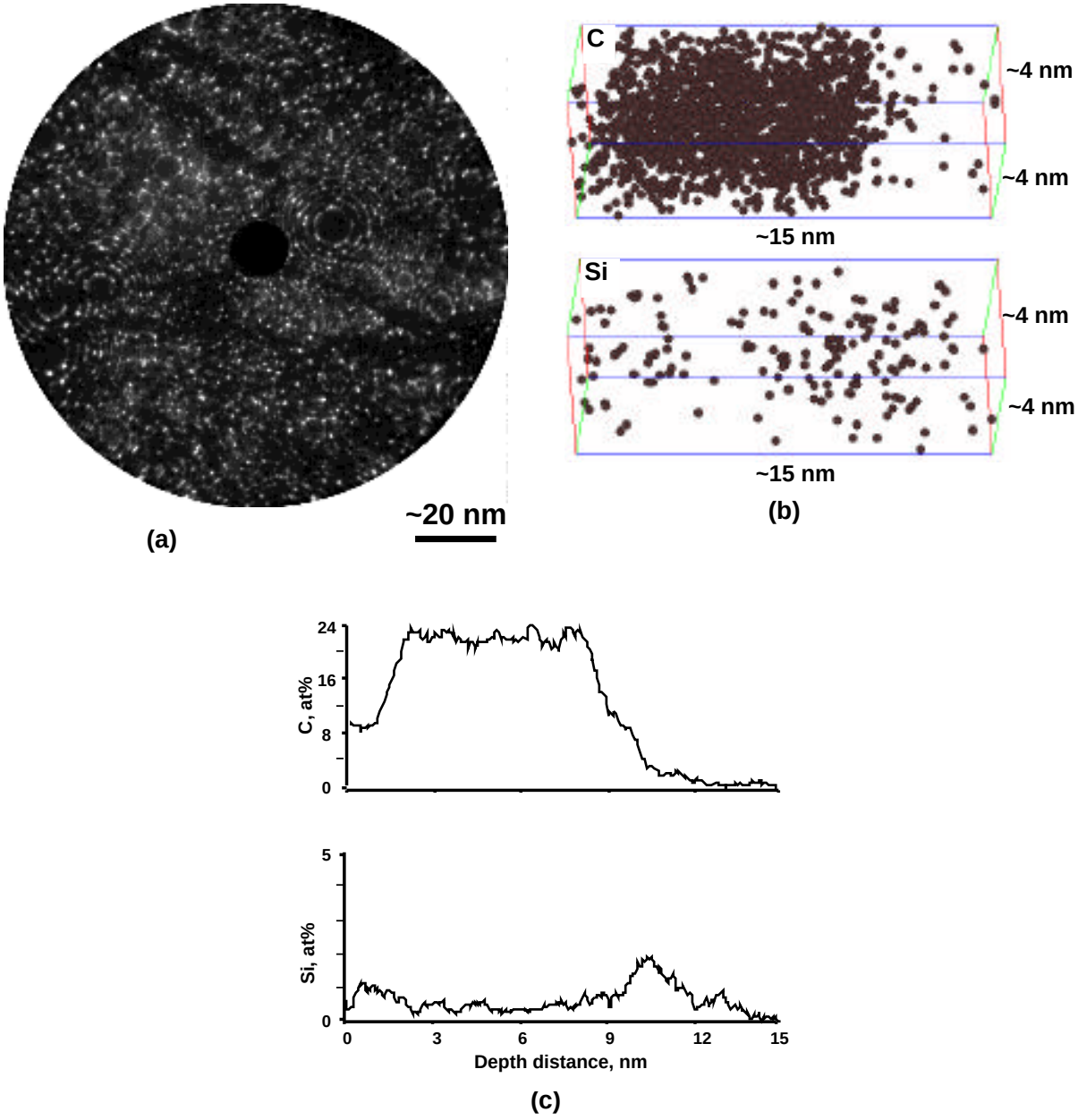

Fig. 12 Pearlitic wire drawn to ε=4.22 and aged at 400°C for 1 hr. (a) Ne field-ion image, (b) 3DAP elemental maps of carbon and silicon, and (c) the corresponding carbon and silicon concentration profiles across the ferrite/cementite interface in (b). Each nanometer of distance roughly corresponds to 1000 atoms.

investigation is not surprising. However, a significantly lower than stoichiometric carbon concentration in deformed cementite is unexpected. The atom probe data indicates the carbon concentration in cementite deformed to a strain of 4.22 is approximately 16 at.%. Indirect evidence for a lower carbon concentration in the cementite after deformation was reported using EELS spectroscopy by Languillaume et al.[11], and recent 3DAP work by Danoix et al.[13] also reported the carbon concentration of the cementite in the deformed pearlitic steel is lower than the stoichiometric value (~20 at.%C). Because stoichiometric cementite was detected in this investigation (in as-patented wire and in wire annealed at or above 400°C), we believe the finding that deformed cementite contains significantly less than the stoichiometric carbon concentration is unequivocal.

Equilibrated cementite has a narrow existence range with respect to carbon concentration[22], so a decrease in the amount of carbon in cementite must be accompanied by the addition of a high density of lattice defects in order to allow a deviation from stoichiometry. Electron microscopy studies by Maurer[5], Gil Sevillano[6] and Inoue[7,8] established cementite lamella in pearlite deformed to somewhat lower strains contain numerous planar defects and slip bands. In this study, the drawing process reduces cementite lamella to

a thickness of about 2 to 5 nm and introduces numerous boundaries between the cementite nanocrystals.

These boundaries, which are defective regions in cementite, can be expected to arise when ferrite and cementite lamella are co-deformed to large strains because the dislocation Burgers vectors in the two phases differ. Reported slip systems in cementite (oP16 structure) at room temperature include (001)[010], (010)[001], and (100)[010] [8], and slip traces have also been seen on the (011), and (110) planes as well[6]. The [010] and [001] cementite Burgers vectors are 0.509 nm and 0.647 nm, respectively, considerably different from the 0.2485 nm Burgers vector in ferrite. There are, however, twelve inter-iron distances in cementite within 5% of a ferrite Burger's vector. Slip along any of these directions amounts to a partial dislocation in cementite. At least some of these additional slip directions must be active or there would not be enough slip systems for ferrite and cementite to deform compatibly. Consequently, the transfer of plastic strain from ferrite to cementite should be accompanied by the creation of stacking faults and vacancies, and at sufficient densities, these defects should allow the carbon concentration in cementite to deviate from stoichiometry. The appearance of occasional amorphous regions along cementite lamella also may be related to the incommensurate Burgers vectors in ferrite and cementite if extensive slip across a ferrite/cementite boundary can produce enough structural disorder to cause amorphization. High strains accompanying mechanical alloying have been shown to produce solid state amorphization of $Fe_{75}C_{25}$ powders[23, 24], so it seems reasonable to expect a 4.22 drawing strain to amorphize some cementite in drawn pearlitic wire.

Although low temperature annealing at 200°C was reported to increase yield strength[16], no noticeable microstructural changes were detected in either ferrite or cementite with TEM and APFIM. The atom probe data do not provide clear evidence of continuing cementite dissolution during annealing at 200°C as Yamada suggested[16]. As the carbon concentration is not uniform in ferrite, quantifying the average carbon concentration in ferrite is not easy. The measured concentration varies greatly from one place to another, and it is thus difficult to conclude whether the carbon concentration in ferrite has increased during annealing at 200°C. It seems more likely that the increase in yield strength accompanying annealing at 200°C results from the locking of mobile dislocations by carbon atoms in ferrite.

Annealing at 400 and 500°C causes substantial changes in the microstructure and distribution of carbon, and these changes readily explain the drop in the strength of drawn wire[14]. The scale of the microstructure coarsens as cementite spherodizes, the spacing of the prior cementite lamella increases, and the ferrite recovers and recrystallizes. All of these microstructural changes lead to a decrease in the resistance to plastic flow. The return of the carbon concentration in ferrite to the pre-deformation level removes any solid-solution strengthening that might have resulted from carbon in the as-drawn ferrite.

Previous studies of the role of silicon during annealing of drawn pearlitic wire showed Si increases the resistance to softening at high annealing temperatures by suppressing spherodization of cementite lamella[14, 15, 18]]. From the present investigation, it appears that this beneficial effect of Si is related to its tendency to segregate to the ferrite/cementite boundaries during annealing, even at temperatures as low as 200°C. Once a layer of excess silicon develops at ferrite/cementite boundaries, the break-up of cementite during spherodization can be expected to be controlled by the relatively sluggish diffusion of silicon.

V. CONCLUSIONS

1. The cementite lamella in pearlitic wire drawn to a strain of 4.22 is polycrystalline with grains as small as 2-5 nm. Some amorphized cementite is found in regions with the smallest interlamellar spacing, but most of the cementite is crystalline.
2. The carbon concentration in ferrite in drawn wire (ε=4.22) is significantly higher than the equilibrium solubility of carbon in ferrite. The carbon distribution in ferrite is not uniform and ranges from 0.2 to 3 at.%. Heterogeneous dissolution of carbon in ferrite suggests that carbon is segregated to dislocations or dislocation pile-ups.
3. Heavy deformation during wire drawing decreases the carbon concentration in cementite significantly (to ~16 at.%).
4. Si is segregated at ferrite/cementite interfaces in as-patented wire. Heavy deformation during cold drawing apparently produces enough mechanical mixing to remove much of the segregation.
5. Annealing at 200°C does not cause any detectable change in the TEM microstructure nor the chemical distribution observed by APFIM despite the fact this heat treatment is reported to increase the yield strength. Thus, the increase in strength accompanying annealing at 200°C is concluded to result from the locking of mobile dislocations by carbon atoms in ferrite.
6. Annealing at 400°C and 500°C changes the microstructure drastically: cementite spherodizes, ferrite recovers and recrystallizes. The carbon concentrations in cementite and ferrite return to the same values as in undeformed pearlite.

ACKNOWLEDGMENTS

This work was partially supported by the Frontier Research Center for Structural Materials at the National Research Institute for Metals and the International Joint Research Grant by NEDO. M. H. Hong gratefully acknowledge the Japan Science and Technology Agency for the JST fellowship, and W. T. Reynolds acknowledges United States National Science Foundation (DMR 9303518

and INT 9600383) for financial support. The authors thank K. Tsuzaki and T. Takahashi for valuable discussions, and M. Murayama for assistance with the APFIM experiments and data analysis.

REFERENCES

1. H. G. Paris: Metallurgy, Processing and Applications of Metal Wires, H. G. Paris and D. K. Kim ed., TMS, Warrendale, PA, 1996, pp. 3-15.
2. J. D. Embury and R. M. Fisher: *Acta Metall*., 1966, vol. 14, pp. 147-59.
3. G. Langford, *Metall. Trans*. 1977, vol. 8A, pp. 861-75.
4. W. J. Nam and C. M. Bae; *Mater. Sci. and Eng. A,* 1995, vol. 203, pp. 278-85.
5. K. Maurer and D. H. Warrington, *Phil. Mag*., 1967, vol. 15, pp. 321-27
6. J. Gil Sevillano: Material Sci. and Eng., 1975, vol. 20, pp. 221-25.
7. A. Inoue, T. Ogura, and T. Masumoto: *Scripta Metal.*, 1976, vol. 11, pp. 1-5.
8. A. Inoue, T. Ogura, and T. Masumoto: *Trans. JIM*, 1977, vol. 17, pp. 149-57.
9. K. Van Acker, J. Root, P. Van Houtte and E. Aernoudt: *Acta Mater*., 1996, vol. 44, pp. 4039-49.
10. D. A. Porter, K. E. Easterling, and G. D. W. Smith: *Acta Metall*., 1978, vol. 26, pp. 1405-22.
11. J. Languillaume, G. Kapelski, and B. Baudelet: *Acta Mater*., 1997, vol. 45, pp. 1201-12.
12. A. R. Waugh, S. Paetke, and D. V. Edmonds: *Metallography*, 1981, vol. 14, pp. 237-51.
13. F. Danoix, X. Sauvage, D. Julien, and J. Copreaux: *Mater. Sci. Eng. A*, 1998, in press.
14. T. Tarui, T. Takahashi, S. Ohashi, and R. Uemori: *Iron and Steelmaker*, 1994, vol. 21, pp. 25-30.
15. T. Tarui, T. Takahashi, H. Tashiro, and S. Nishida: Processing and Applications of Metal Wires, H. G. Paris and D. K. Kim ed., TMS, Warrendale, PA, 1996, pp. 87-96.
16. H. G. Read, W. T. Reynolds Jr., K. Hono, and T. Tarui: *Scripta Meter*., 1997, vol. 37, pp. 1221-30.
17. Y. Yamada: *Trans. ISIJ*, 1976, vol. 16, pp. 417-26.
18. V. N. Gridnev, V. V. Nemoshkalenko, Yu. Ya. Meshkov, V. G. Gavrilyuk, V. G. Prokopenko, and O. N. Razumov: *Phys. Stat. Sol. A*, 1975, vol. 31, pp. 201-210.
19. K. Makii, H. Yaguchi, M. Kaiso, N. Ibaraki, Y. Miyamoto , and Y. Oki: *Scripta Mater.*, 1997, vol. 37, pp. 1753-59.
20. H. Suto and T. Kudo: *J. Jap. Inst. Met.*, 1972, vol. 36, pp. 693-701.
21. D. Blavette, B. Deconihout, A. Bostel, J. M. Sarrau, M. Bouet, and A. Menand: *Rev. Sci. Instrum.*, 1993, vol. 64, 2911-19.
22. F. X. Kayser and Y. Sumitomo: *J. Phase Equilibria*, 1997, vol. 18, no. 5, pp. 458.
23. T. Nasu, C. C. Koch, K. Nagaoka, N. Itoh, M. Sakurai, and K. Suzuki: *Mater. Sci. Eng. A*, 1991, vol A134, pp. 1385-88.
24. T. Tanaka, T. Nasu, K. N. Ishihara, and P. H. Shingu: *J. Less-Comm Metals*, 1991, vol 171, pp. 237-47.